Spin-polarized electronic current induced by sublattice engineering of graphene sheets with boron/nitrogen

Hyoungki Park, Amita Wadehra, John W. Wilkins, and Antonio H. Castro Neto

Phys. Rev. B **87**, 085441 — Published 27 February 2013

DOI: 10.1103/PhysRevB.87.085441

Half-metallic electronic structure induced by sublattice engineering of graphene sheets with boron/nitrogen

Hyoungki Park,* Amita Wadehra, and John W. Wilkins
Department of Physics, The Ohio State University, Columbus, Ohio 43210, USA

Antonio H. Castro Neto
Graphene Research Centre, National University of Singapore, Singapore 117542 and
Department of Physics, Boston University, Boston, MA 02215, USA
(Dated: February 14, 2013)

Abstract: We show that spin-polarized electron transport can be achieved by the substitutional doping of only one sublattice of graphene by nitrogen or boron atoms. The bipartite character via two sublattices remains persistent in the electronic structures of graphene doped with low concentrations of nitrogens (borons). The delocalized spin-densities induced by the unpaired electrons at substitutional sites permeate only through the sublattice where the nitrogen (boron) atoms belong. For interacting nitrogen (boron) atoms located along the "zigzag" direction and in the same sublattice the ferromagnetic spin-ordering is favorable, and substitution-induced localized impurity states selectively disturb the spin-polarized π-orbital of that same sublattice. The bipartite character of graphene lattice governs the unique properties of 2D hybrid graphene-boron nitride nanostructures.

Half-metallicity, the asymmetric electron transport for the different electron spin projections, could have a significant effect on the future spin-based electronic devices. Substantial efforts have been made to search for materials with this property since it was first proposed[1]. Recent developments of two-dimensional (2D) nanomaterials hold promise for realizing such exotic systems. One such material is graphene, an atomically thin layer of carbon atoms arranged in a bipartite honeycomb lattice, that has attracted a lot of interest because of its intriguing physics as well as its application potential.[2,3] The semiconducting properties in graphene can be controlled by doping and gating, which allows flexibility in design and optimization of graphene-based devices. Previous experimental and theoretical studies report that half-metallicity can be achieved in graphene nanoribbons under applied electric field or with chemical modifications[4–8]. Here, using a hybrid exchange-correlation functional in density functional theory (DFT), we show that boron/nitrogen-doped graphene sheets can become half-metallic by selectively engineering the spin-polarized electronic structure of only one of the two sublattices of the 2D honeycomb lattice. We also show how the distinct modulation of the two sublattices, due to different concentrations and configurations of boron and nitrogen substitutions (as hexagonal boron nitride, h-BN), influences the electronic structure of the 2D hybrid graphene-boron nitride (2D-BCN) materials. These 2D-BCN nanostructures show a rich variety of physical properties, distinct from parent materials, and offer numerous possible technological applications.[9–15].

There has been an increasing interest lately in exploring spintronic devices based on graphene. Although pristine graphene is nonmagnetic, yet various theoretical studies show that magnetism can be induced in graphene by incorporating defects such as vacancies, adatoms and substitutional atoms.[16–18] The experimental evidence, on the other hand, is scarce and controversial. On the basis of our extensive spin-polarized calculations on this system, we deduce that the calculated magnetic moments are highly sensitive to the exchange-correlation functional and the choice of k-point mesh used for the calculation. Spin-DFT calculations with functionals based on local density approximations such as PBE (Perdew-Burke-Ernzerhof)[19] yield zero spin-splitting between spin-up and spin-down bands, and consequently non-magnetic solution for an isolated as well as two interacting nitrogen substitutions on same sublattice in graphene. Moreover, k-point sampling is crucial to capture the extent of spin-splitting and dispersion of the bands near the K-point; the convergence of magnetic moment with increasing number of k-points should be carefully monitored since it is independent of the size of the computational cell and the convergence of energy. In this work we use the Heyd-Scuseria-Ernzerhof (HSE)[20–22] hybrid functional to accurately study the spin-polarized electronic structures of hybrid BCN nanostructures.

We begin with a comprehensive and systematic hybrid-DFT study of magnetism in graphene containing substitutional nitrogen atoms, with an aim to investigate its suitability for spintronic devices. The symmetry of the two sublattices of the 2D honeycomb lattice is intertwined with the spin states and governs fundamental properties of nitrogen-doped graphene. Our results reveal that the interacting substitutional-atoms residing on the same sublattice favor the ferromagnetic (FM) spin-alignment for their local unpaired electrons, and substitution-induced impurity states predominantly disturb the spin-polarized π-orbital of the sublattice where the substitutional atoms belong. The final result is an asymmetric electron transport for the different spin states. Such asymmetric electron transport and the possibility of achieving complete spin-polarization for the transport carrier may hold the key to the feasibility of spin-based devices.

Nitrogen has an extra electron than carbon, and

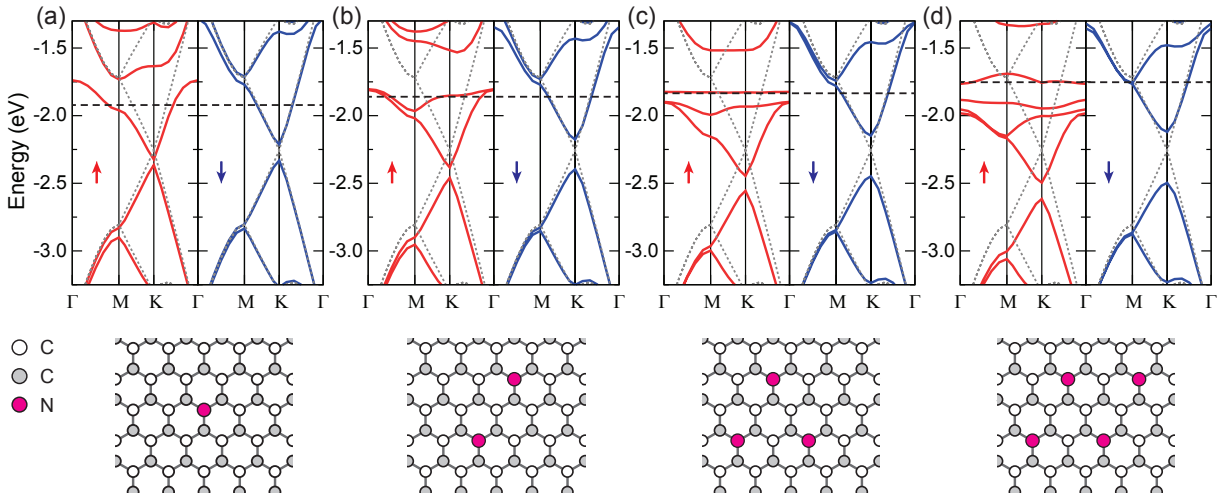

FIG. 1. (color online) Spin-polarized band structures of (a) single, (b) two, (c) three, and (d) four nitrogen impurities in graphene reveal the asymmetric electron transport for the spin-up (red lines) and spin-down components (blue lines). The dotted gray lines correspond to the band structure of pristine graphene. In (a), partial occupation of both spin-up and spin-down components of the hybridized impurity band results in a small net magnetic moment. In (b), two impurity bands are observed for the two substitutional N atoms. The lower hybridized band for spin-up component is almost fully occupied, whereas the localized upper band shows partial occupation. A "spin-down" pocket is formed due to partial occupation of the spin-down component of the hybridized impurity band. Similar behavior is observed for (c) three and (d) four nitrogen impurities in graphene. Gating and consequent shifting of the Fermi level upwards would enable transport exclusively through spin-down component, a clear signature of half-metallicity, whereas transport through spin-up component would be forbidden due to large gap.

is comparable in size. Figure 1 shows spin-resolved band structures for up to four nitrogen substitutions in graphene. In Fig. 1(a), substituting a carbon atom in a 200-atom graphene supercell with a nitrogen atom introduces an unpaired electron, and induces an impurity state. Our spin-polarized HSE-DFT calculations show that the excess charge introduced by N atom is unevenly occupied between the two spin channels. An exchange spilitting of 0.5 eV is observed, with the majority spin channel lying lower in energy by 0.5 eV as compared to the minority spin channel. This is in strong contrast with the zero spin-splitting from PBE calculations, and leads to quite asymmetric electronic structures between spin-up and spin-down configurations.

In the spin-up band structure of Fig. 1(a), the impurity state greatly disturbs the graphene band structure near the Fermi level by hybridizing with the delocalized π^*-orbital of graphene. On the other hand, the spin-down impurity state lies about 0.5 eV above the spin-up state and deep in the conduction band of graphene. The spin-down state hybridizes with graphene states along all the high-symmetry k-points, and induces a gap at the "Dirac point" by breaking the graphene symmetry. However, the spin-down electronic structure of graphene near the Fermi level is hardly affected by the substitution with a nitrogen atom. The unpaired electron raises the Fermi level and both spin-up and spin-down components of the hybridized band lie below the Fermi level, leading to small net magnetic moment induced by the unpaired electron. The effect on transport comes from a change in the effective mass, m^*_σ, for the two spin species, $\sigma = \uparrow, \downarrow$, since the Fermi velocity (v_F) becomes spin dependent: $m^*_\sigma \approx E_F/v^2_{F,\sigma}$.

Substitution of two carbon atoms by nitrogen atoms, belonging to the same sublattice of graphene and separated along the "zigzag" direction, results in two impurity bands with distinct characteristics in the spin-up band structure of Fig.1(b). One of the impurity bands hybridizes with graphene π^*-orbital and shows similar features as that for the single nitrogen substitution discussed above. The other impurity band (i) displays more localized features throughout, (ii) cuts through the conduction bands of graphene, and (c) opens up a sizable gap, ~0.25 eV, near the Fermi level. The spin-splitting lifts the hybridized bands of spin-down component, so they lie higher in energy than the spin-up component. However, near the K-point, the hybridized spin-down band still maintains the π^*-band character of the pristine graphene, and has lower energy than the spin-up component of the localized band near the Fermi level. Thus, a "spin-down pocket" is created around the K-point, resulting in a loss of net magnetic moment from $2\mu_B$. Similar characteristics for the bands are observed for the three and four nitrogen substitutions, Fig.1(c) and (d), in our 200-atom graphene supercells. Increasing the number of substitutions stacks up more localized bands in the spin-up band structure, but the spin-down bands near the Fermi level remain fairly unaffected by the substitutions. This asymmetric alteration of electronic structure near the Fermi level between spin-up and

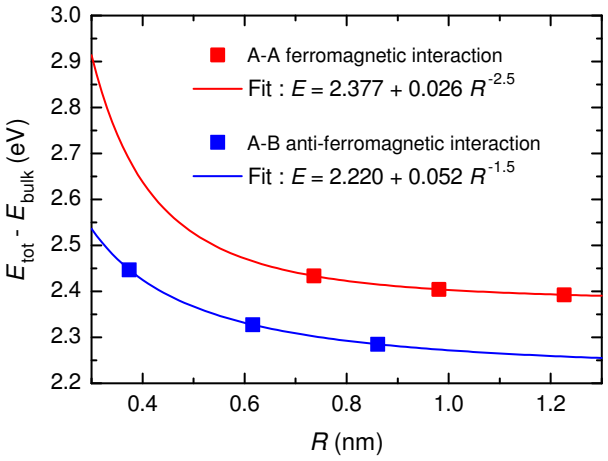

FIG. 2. (color online) Energetic trends of two interacting N atoms as function of their separation R. When two N atoms in the same sublattice, the ground state spin-configuration is ferromagnetic and its trend is represented in red. On the other hand, the trend in blue is for the anti-ferromagnetic spin-configuration, which is the ground state for two N atoms in different sublattices. The ferromagnetic interaction falls off as $1/R^{2.5}$, and the anti-ferromagnetic interaction decays as $1/R^{1.5}$. All energies are shifted relative to the energy of pristine graphene.

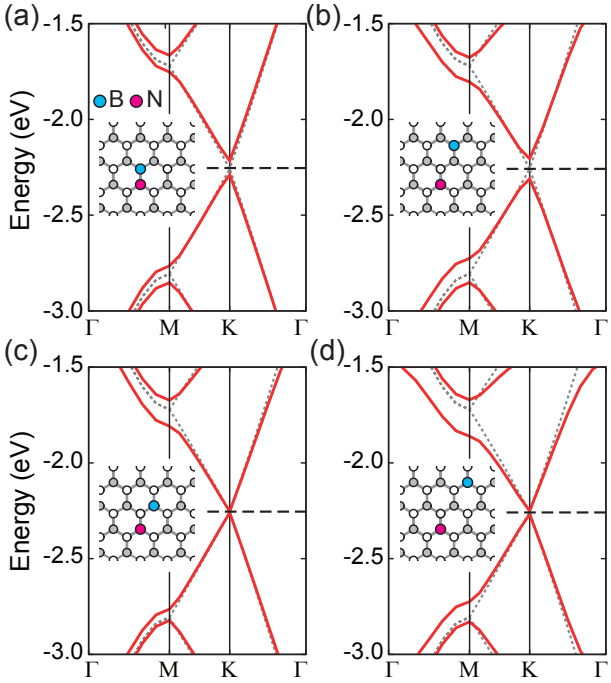

FIG. 3. (color online) Band structures of graphene with a low concentration of boron and nitrogen atoms substituting carbon atoms, $C_{0.99}(BN)_{0.01}$. In (a) and (b), the two substituting atoms are at different sublattice sites of graphene, disturbing π-orbitals of both K- and K'-points in the Brillouin zone of graphene and inducing gaps of 0.07 eV and 0.1 eV for (a) and (b), respectively. In (c) and (d), on the other hand, the two substituting atoms occupy sites of the same sublattice, leaving the π-orbital system of the other sublattice less affected by substitutions. In all plots, the dotted gray lines represent bands of pristine graphene whereas those for BCN structures are shown by solid red lines.

spin-down states with increasing number of substitutions yields a higher net magnetic moment and a bigger gap between the top-most localized impurity band and the band just above it in the spin-up band structure. Due to the existence of "spin-down pocket" the Fermi level is not within the gap induced by impurity states, but close to the top-most impurity state in the spin-up band structure. Hence, shifting the Fermi level up in the gap by gating can make the spin-down component as the only channel available for carrier transport, i.e., half-metallic transport.

The ferromagnetic spin-alignment for the unpaired electrons localized at substitutional sites is requisite to produce the half-metallic electronic structure. We find that the ferromagnetic spin-ordering is energetically favorable when all nitrogen atoms are at the same sublattice, and when they are separated more than 0.3 nm along the "zigzag" direction. To elucidate the nature of the magnetic coupling of N atoms we study energetic trends of two interacting N atoms as function of their separation in our 200-atom computational cell. When the separation is relatively large (greater than 0.3 nm), the ground state spin-configuration is ferromagnetic with $E_{\rm AFM} - E_{\rm FM} \sim 50$ meV for two substitutional atoms on the same sublattice, but anti-ferromagnetic (AFM) with $E_{\rm FM} - E_{\rm AFM} \sim 150$ meV between atoms on different sublattices. This long-range spin-interaction can be explained within the Ruderman-Kittel-Kasuya-Yosida (RKKY) approximation, an indirect exchange interaction mediated by the conduction electrons of a host medium.[23–25] Figure 2 shows the ferromagnetic and the anti-ferromagnetic energetic trends for two N atoms on the same sublattice and different sublattices, respectively. In both cases, the interaction strength decays with increasing separation R. The inverse power law fit indicates that the ferromagnetic interaction falls off as $1/R^{2.5}$, faster than $1/R^{1.5}$ for the anti-ferromagnetic interaction. Although the range of our data is very limited due to computational expense, our results are in general agreement with previous analytical and numerical studies of RKKY interaction in graphene.[26–31] Hence, the RKKY is the dominant magnetic coupling interaction that induces the ferromagnetic spin-alignment for configurations with half-metallic electronic structures in Fig.1. When the separation is shorter than 0.3 nm, the magnetic coupling cannot be interpreted simply by the RKKY interaction due to the strong direct interaction between the nitrogen atoms. Another important observation is that the substitution of carbon atoms by boron atoms shows qualitatively similar results as the nitrogen case. Impurity states induced by substitutional boron atoms act as acceptor states and locate lower in the band structure than the donor-like states from nitrogen atoms, and they hy-

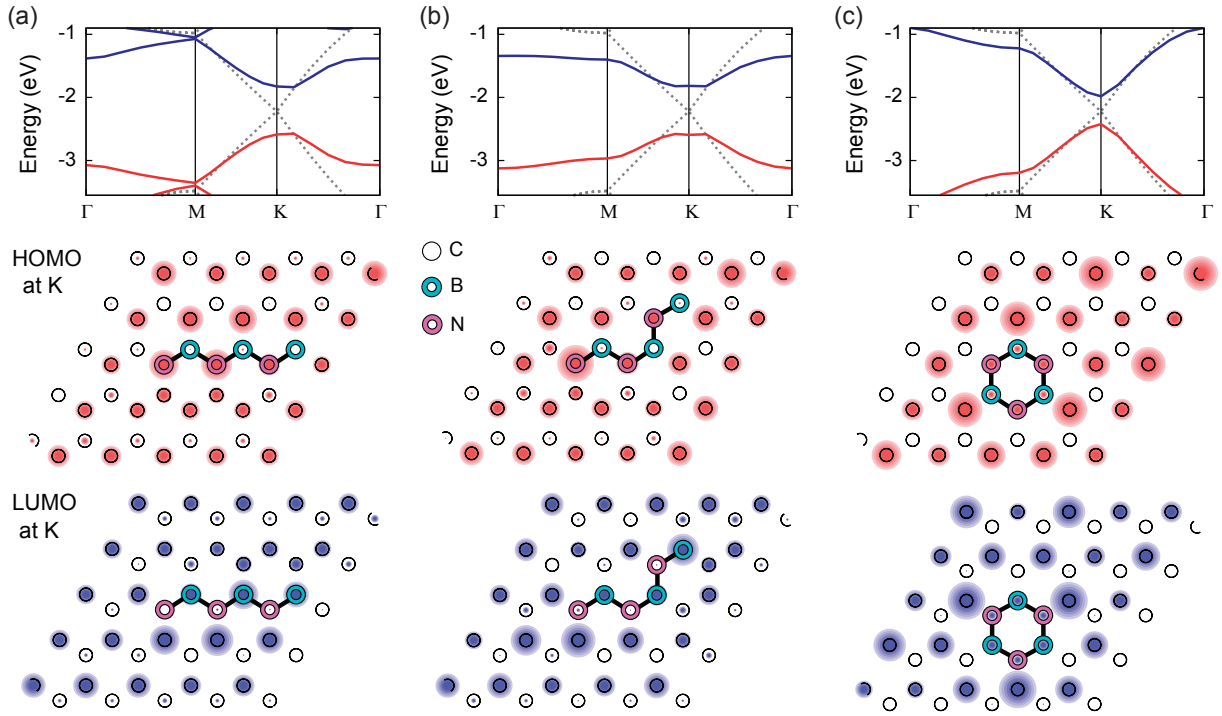

FIG. 4. (color online) Band structures (top) and site-projected wavefunction characters at the high symmetry K-point superimposed on the $C_{0.88}(BN)_{0.12}$ structures for the topmost valence band (middle) and lowermost conduction band (bottom). The BN pairs are arranged as, in increasing order of stability: (a), zigzag-chain, (b), armchair-chain, and (c), hexagonal-ring configurations. For figures in the middle (bottom) row, the size of red (blue) shading at each atomic position corresponds to the relative amount of contributions from the p_z-orbital of the atom to the topmost valence band (lowermost conduction band) at K-point.

bridize with the graphene π-orbital instead of the π^*-orbital. Nevertheless, overall conclusion is the same as in the nitrogen case. Having the bipartite electronic structure interwoven with spin states via two sublattices is crucial for realization of half-metallicity in these doped graphene systems.

For the rest of paper we investigate how the bipartite electronic structure of graphene is affected by the introduction of substitutional boron and nitrogen atoms. In particular, we study how various arrangements of boron and nitrogen atoms for different concentrations modulate the bipartite sublattices and influence properties of these 2D-BCN structures.

The bipartite character of graphene lattice is evident in the BCN systems containing low concentrations of boron and nitrogen. Figure 3 shows that just a pair of B and N, as BN, when occupying adjacent but different sublattice sites in our 200-atom graphene supercell disturbs π-orbitals of both K- and K′-points in the Brillouin zone of graphene and opens up the gap of 0.07 eV in pristine graphene. The band gap further increases to 0.1 eV when B and N are located far apart but still occupy different sublattice sites as shown in Fig. 3(b). However, when B and N are located on the sites belonging to the same triangular sublattice, the π-orbital system of only that sublattice is affected. Consequently, there is an order of magnitude smaller band gap opening, 0.006–0.01 eV, for such substitutions in Fig. 3(c) and (d). The electronic structures of all these BCN hybrid systems near the Fermi level result from the hybridization of impurity states of substituting atoms and graphene bands. Energetically, the atomic configuration with the formation of a BN pair, Fig. 3(a), is the most stable. Increasing separation between boron and nitrogen atoms from the pair formation raises the total energy by more than 1 eV.[10]

Proceeding to a little higher concentration of BN substitutions in graphene, we investigate three different configurations for the BCN system containing three BN moieties in 50-atom supercell. Figure 4 displays band structures (top) and site-projected wavefunction characters at the high symmetry K-point superimposed on the $C_{0.88}(BN)_{0.12}$ structures for the topmost valence band (middle) and lowermost conduction band (bottom) for zigzag-chain, armchair-chain, and hexagonal ring configurations. The formation energies for zigzag-chain, armchair-chain and hexagonal ring are 5.06 eV, 4.90 eV, and 3.75 eV, respectively, making the hexagonal ring the most stable configuration. Both zigzag- and armchair-chain BN configurations disturb the graphene symmetries at all the high symmetry points and show similar gaps of ∼1.7 eV and ∼0.7 eV at Γ- and K-point, respectively. The periodic image distance of BN chains is closer in Fig. 4(a), leading to more dispersed impurity bands than in Fig. 4(b). The highly symmetric BN

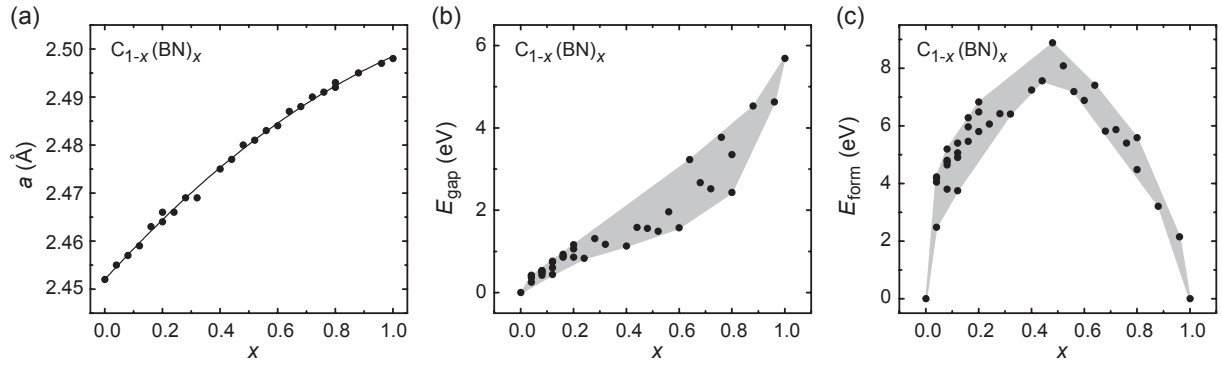

FIG. 5. Selected properties as a function of BN concentration in 2D-BCN structures. (a), Lattice constant, (b), band gap, and (c), formation energy versus concentration of BN, x. The properties at $x = 0$ and $x = 1$ are those of pure graphene and pure h-BN, respectively. The dots are the values obtained for the BCN systems at a given concentration and the line/shading is guide to the eye. Multiple dots for a given concentration indicate that more than one configuration (armchair chains, zigzag chains, hexagonal rings, random distributions) are studied. Relaxed lattice constants follow a tight quadratic trend in (a). Band gaps and formation energies, however, are sensitive to the type of configuration and can show large variation, as depicted by the shading in (b) and (c). There is a peak in the formation energy at $x \sim 0.5$.

hexagonal ring configuration Fig. 4(c) opens a gap of 0.44 eV at the K-point, but maintains the graphene-like electronic structure in the proximity of the Fermi level. As a manifestation of bipartite nature of the sublattices in graphene, p_z-orbitals of all the atoms in one of the sublattices equally contribute to the topmost valence band, the π-band, at K-point, and atoms in the other sublattice contribute to the lowermost conduction band, π*-band. In Fig. 4(a) and Fig. 4(b), this sublattice-symmetry is slightly impaired in the proximity of BN clusters, but still remains persistent overall. On the other hand, the bipartite character of graphene sublattices is fully preserved in hexagonal configuration. Consequently, atoms in the BN hexagonal ring and carbon atoms in the other sublattice rarely contribute to the topmost valence band and the lowermost conduction band. This holds for all the configurations that we study with multiple BN hexagonal rings in graphene, and implies that the electric transport is mainly through the carbon network when BN hexagonal rings are embedded in graphene. This shows the distinct roles of the two graphene sublattices in determining electronic and transport properties for different configurations of such nanosystems.

Figure 5 summarizes our results for the variation in average lattice constant, band gap, and formation energy as a function of BN concentration, x, in the 50-atom supercells of BCN structures. We calculated the formation energy of a given system as $E_{\rm form} = E_{\rm tot} - (N_{\rm C}/50) \cdot E_{\rm C}^{\rm bulk} - (N_{\rm BN}/25) \cdot E_{\rm BN}^{\rm bulk}$. We have plotted properties for many possible configurations (armchair chains, zigzag chains, hexagonal rings, random distributions) at a given concentration, as indicated by multiple data points. A quadratic trend is observed for lattice constants while large variation in band gaps and formation energies, depending on the configuration, is observed. The formation energy shows a peak at $x \sim 0.5$. In agreement with experimental observations[9], a strong tendency to form domains exists both for low concentrations of BN in graphene, and low concentrations of carbon atoms in h-BN. Consequently, structures containing pairs or clusters of substituting atoms are energetically favored over randomly distributed atoms, as evident also from Fig. 3. The formation energies are always lower for structures having BN or carbon hexagonal rings than those containing open chains, as also shown in Fig. 4.

We use the planewave projector augmented-wave (PAW) method[32] with the HSE06 hybrid functional in the VASP code.[33–35] We use a planewave energy cutoff of 700 eV for all our calculations. The hybrid BCN nanostructures are modeled in 50 atom and 200 atom supercells, $5 \times 5 \times 1$ and $10 \times 10 \times 1$ of the two atom unitcell, respectively. The Brillouin zone (BZ) integration for graphene and the single-layer h-BN is performed on a Γ-centered $10 \times 10 \times 1$ k-point meshes, and equivalent meshes are used for all the simulation cells. Band structures are computed on discrete k-point meshes along high symmetry directions: Γ-M-K-Γ.

To summarize, the bipartite character of graphene lattice and its alteration is significantly responsible for the unique electronic and magnetic properties of nitrogen- and/or boron-doped graphene. We demonstrate that ferromagnetism can be achieved in doped graphene sheets when the substituent atoms are all located along zigzag direction and occupy sites belonging to the same sublattice. The resultant asymmetric electron transport along spin-up and spin-down states facilitates the observance of half-metallicity in these systems. We also elaborate on the role of the two sublattices in determining the stability and electronic structures of a variety of 2D-BCN nanostructures.

This work was supported by DOE-BES-DMS (DE-FG02-99ER45795). We used computational resources of the NERSC, supported by the U.S. DOE (DE-AC02-05CH11231), and the Ohio Supercomputing Center.

AHCN acknowledges DOE grant DE-FG02-08ER46512, ONR grant MURI N00014-09-1-1063 and the NRF-CRP award "Novel 2D materials with tailored properties: beyond graphene" (R-144-000-295-281).

* Correspondence author: hkpark@mps.ohio-state.edu

[1] R. A. de Groot, F. M. Mueller, P. G. van Engen, and K. H. J. Buschow, Phys. Rev. Lett. **50**, 2024 (1983).
[2] A. H. Castro Neto, F. Guinea, N. M. R. Peres, K. S. Novosolev, and A. K. Geim, Rev. Mod. Phys. **81**, 109 (2009).
[3] A. K. Geim and K. S. Novosolev, Nat. Mat. **6**, 183 (2007).
[4] Y. W. Son, M. L. Cohen, and S. G. Louie, Nature **444**, 347 (2006).
[5] M. Wu, X. Wu, Y. Gao, and X. C. Zeng, Appl. Phys. Lett. **94**, 223111 (2009).
[6] Y. Liu, X. Wu, Y. Zhao, X. C. Zeng, and J. Yang, J. Phys. Chem. C **115**, 9442 (2011).
[7] J. M. Pruneda, Phys. Rev. B **81**, 161409(R) (2010).
[8] Y. Ding, Y. Wang, and J. Ni, Appl. Phys. Lett. **95**, 123105 (2009).
[9] L. Ci, L. Song, C. Jin, D. Jariwala, D. Wu, Y. Li, A. Srivastava, Z. F. Wang, K. Storr, L. Bacilas, et al., Nat. Mat. **9**, 430 (2010).
[10] H. Park, A. Wadehra, J. W. Wilkins, and A. H. Castro Neto, Appl. Phys. Lett. **100**, 253115 (2012).
[11] J. Li and V. B. Shenoy, Appl. Phys. Lett. **98**, 013105 (2011).
[12] A. Ramasubramaniam, D. Naveh, and E. Towe, Nano Lett. **11**, 1070 (2011).
[13] B. Xu, Y. H. Lu, Y. P. Feng, and J. Y. Lin, J. Appl. Phys. **108**, 073711 (2010).
[14] Y. Fan, M. Zhao, Z. Wang, X. Zhang, and H. Zhang, Appl. Phys. Lett. **98**, 083103 (2011).
[15] K. Venu, S. Kanuri, K. Raidongia, K. P. S. S. Hembram, U. V. Waghmare, and R. Datta, Sol. State Commun. **150**, 2262 (2010).
[16] O. V. Yazyev, Rep. Prog. Phys. **73**, 056501 (2010).
[17] O. V. Yazyev and L. Helm, Phys. Rev. B **75**, 125408 (2007).
[18] O. V. Yazyev and M. I. Katsnelson, Phys. Rev. Lett. **100**, 047209 (2008).
[19] J. P. Perdew, K. Burke, and M. Ernzerhof, Phys. Rev. Lett. **77**, 3865 (1996).
[20] J. Heyd, G. E. Scuseria, and M. Ernzerhof, J. Chem. Phys. **118**, 8207 (2003).
[21] J. Heyd and G. E. Scuseria, J. Chem. Phys. **121**, 1187 (2004).
[22] J. Heyd, G. E. Scuseria, and M. Ernzerhof, J. Chem. Phys. **124**, 219906 (2006).
[23] M. A. Ruderman and C. Kittel, Phys. Rev. **96**, 99 (1954).
[24] T. Kasuya, Prog. Theor. Phys. **16**, 45 (1956).
[25] K. Yosida, Phys. Rev. **106**, 893 (1957).
[26] S. Saremi, Phys. Rev. B **76**, 184430 (2007).
[27] A. M. Black-Schaffer, Phys. Rev. B **81**, 205416 (2010).
[28] M. Sherafati and S. Satpathy, Phys. Rev. B **83**, 165425 (2011).
[29] J. Kang, H.-X. Deng, S.-S. Li, and J. Li, J.Phys: Condens. Matter **23**, 346001 (2011).
[30] S. R. Power, F. S. M. Guimaraes, A. T. Costa, R. B. Muniz, and M. S. Ferreira, Phys. Rev. B **85**, 195411 (2012).
[31] H. Lee, E. R. Mucciolo, G. Bouzerar, and S. Kettemann, Phys. Rev. B **86**, 205427 (2012).
[32] P. E. Blochl, Phys. Rev. B **50**, 17953 (1994).
[33] G. Kresse and J. Furthmuller, Phys. Rev. B **54**, 11169 (1996).
[34] G. Kresse and D. Joubert, Phys. Rev. B **59**, 1758 (1999).
[35] J. Paier, M. Marsman, K. Hummer, G. Kresse, I. Gerber, and J. Angyan, J. Chem. Phys. **124**, 154709 1 (2006).